

# Three-Dimensional Imaging and Processing Using Computational Holographic Imaging

YANN FRAUEL, THOMAS J. NAUGHTON, OSAMU MATOBA, ENRIQUE TAJAHUERCE, AND  
BAHRAM JAVIDI

## *Invited Paper*

*Digital holography is a technique that permits digital capture of holograms and subsequent processing on a digital computer. This paper reviews various applications of this technique. The presented applications cover three-dimensional (3-D) imaging as well as several associated problems. For the case of 3-D imaging, optical and digital methods to reconstruct and visualize the recorded objects are described. In addition, techniques to compress and encrypt 3-D information in the form of digital holograms are presented. Lastly, 3-D pattern recognition applications of digital holography are discussed. The described techniques constitute a comprehensive approach to 3-D imaging and processing.*

**Keywords**—*Computational holographic imaging, three-dimensional data compression, three-dimensional image encryption, three-dimensional image processing, three-dimensional object recognition.*

## I. INTRODUCTION

Three-dimensional (3-D) imaging has had a long history (see, for instance, [1] and [2]). However, it is only recently that technological advances have permitted the application of effective techniques [3]. Digital holography is one of these techniques. It is derived from conventional holography but uses a digital camera instead of a photographic medium in order to capture the holograms [4]–[23]. The development

of this technique was made possible by advancements in charge-coupled device (CCD) and CMOS image sensor technology. An advantage of digital holography is that the hologram is directly obtained in digital form. There is no need for an analog recording of the hologram and the corresponding chemical or physical development.

A hologram records the interference pattern obtained from the superposition of a reference beam and the beam scattered by an object [24]. The 3-D information about the object is contained in the phase of the object beam. Following the principle of interferometry, this information is present in the intensity of the hologram that is captured by the camera. Today, the size of the pixels in available digital cameras is usually not less than a few micrometers. This factor limits the maximum spatial frequency of the interference pattern and therefore prevents the use of a large angle between the object and the reference beams. Actually, it is practically necessary to employ an in-line recording configuration, in which the reference beam is parallel to the object beam. However, the problem of this configuration appears when one tries to reconstruct the object from the hologram. Indeed it is not possible to separate the reconstructed object beam from the other diffracted terms. A way to overcome this problem is to use the phase-shift technique, which consists of acquiring several interference patterns with various phase retardations of the reference beam. By digitally combining these interference patterns appropriately, it is possible to recover the complex wave amplitude of the sole object beam [25], [26].

Because digital holograms are directly available in digital form, they can readily be processed. The primary application consists of simulating the inverse propagation of the light using a computer in order to digitally reconstruct the original 3-D object [27]. However, an optical reconstruction is also possible [28]. In addition, digital holograms can be digitally transmitted and the 3-D object can be remotely reconstructed (digitally or optically). Moreover, many types of processing can be applied to digital holograms such as compression—in order to reduce storage space and transmission

Manuscript received April 12, 2005; revised October 3, 2005. The work of T. J. Naughton was supported by Enterprise Ireland and Science Foundation Ireland. The work of E. Tajahuerce was supported by the Convenio Universitat Jaume I-Fundaci Caixa Castelló under Project P1-1B2002-29.

Y. Frauel is with the Department of Computer Science, IIMAS-Universidad Nacional Autónoma de México, México, D.F. 04510, Mexico (e-mail: yann@leibniz.iimas.unam.mx).

T. J. Naughton is with the Department of Computer Science, National University of Ireland, Maynooth, Ireland (e-mail: tom.naughton@nuim.ie).

O. Matoba is with the Department of Computer and Systems Engineering, Kobe University, Kobe 657-8501, Japan (e-mail: matoba@kobe-u.ac.jp).

E. Tajahuerce is with the Departament de Ciències Experimentals, Universitat Jaume I, Castelló 12080, Spain (e-mail: enrique.tajahuerce@uji.es).

B. Javidi is with the Electrical and Computer Engineering Department, University of Connecticut, Storrs, CT 06269-2157 USA (e-mail: bahram@engr.uconn.edu).

Digital Object Identifier 10.1109/JPROC.2006.870704

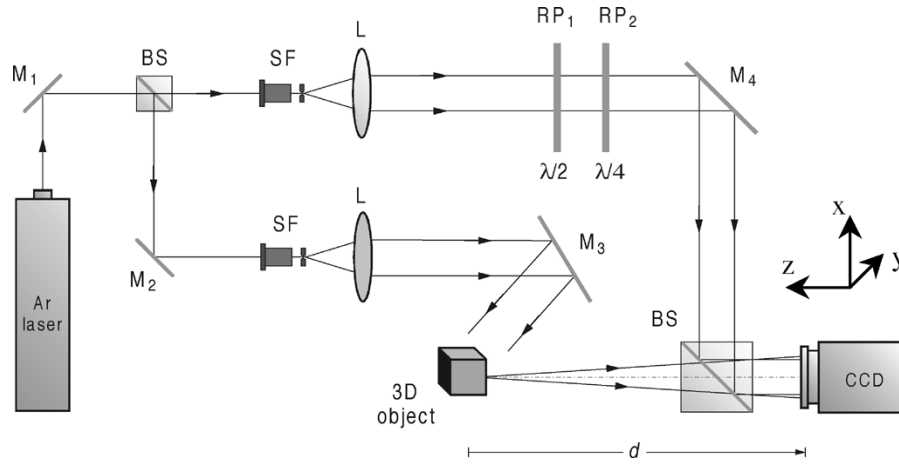


**Fig. 1.** Experimental setup to record a digital hologram. M: mirror; BS: beamsplitter; SF: spatial filter; L: lens; RP: retardation plane.

times [29]–[32]—and encryption—in order to secure or authenticate data [30], [33]–[35]. Lastly, the information contained in digital holograms can also be used to perform 3-D object recognition [27], [36]–[39].

In Section II, we will recall the principles of phase-shift digital holography. Section III will describe the optical and digital reconstruction of 3-D objects from digital holograms. Section IV will be devoted to the compression of digital holograms and Section V to their encryption, either by optical or digital means. Section VI, will present 3-D object recognition techniques using digital holography. Finally, conclusions will be given in Section VII.

## II. PRINCIPLE OF PHASE-SHIFT DIGITAL HOLOGRAPHY

Phase-shift interferometry is one of the techniques used to capture digital holograms [25], [26]. In this technique, the object and the reference beams are directed on axis toward the detector. Several interference patterns between the reference and object waves are recorded. The phase of the reference wave is changed continuously or by steps during the recording. By combining the different recorded interference patterns in a computer, it is possible to obtain the amplitude and phase of the sole object wave.

One way to apply phase-shift techniques in digital holography is by using phase retardation plates [33]. In particular, it is possible to use a half-wave and a quarter-wave plates in the reference beam of a Mach–Zehnder interferometer, as is shown in Fig. 1. In this optical configuration, a laser beam is divided by a beam splitter into an object and a reference beam. Each beam is then expanded and collimated in order to obtain two uniform plane waves traveling in different directions.

The object beam illuminates the 3-D object we want to record. The light scattered by the object travels toward the CCD detector through a second beam splitter. Its complex amplitude distribution in the sensor plane can be written in the form

$$O(x, y, 0) = A_O(x, y) \exp[i\varphi_O(x, y)] \quad (1)$$

where  $A_O(x, y)$  and  $\varphi_O(x, y)$  are the amplitude and phase of the wave, respectively.

The parallel reference beam in Fig. 1 travels through two retarder plates, one quarter- and one half-wave plate, for the implementation of four-step phase-shifting digital interferometry. The light emitted by the laser is linearly polarized. The fast axes of the half- and quarter-wave plates are initially aligned with the laser polarization. This configuration corresponds to a 0 (reference) phase-shift. When the slow axis of the half-wave (respectively, quarter-wave) plate is aligned with the laser polarization, a phase retardation of  $\pi$  (respectively,  $\pi/2$ ) is introduced without modifying the polarization. Thus, by using the four possible configurations of the slow and fast axes of the two plates, it is possible to achieve a phase-shift of  $\Delta\varphi = 0, \pi/2, \pi,$  and  $3\pi/2$  on the reference beam. After being reflected by the second beam splitter, the reference beam interferes with the light diffracted by the 3-D object on the CCD detector. The intensity ratio between the two arms is chosen in a way that the camera collects approximately the same power from the light scattered by the object as from the reference wave. Similar to (1), the complex field of the reference wave can be written as

$$R_{\Delta\varphi}(x, y, 0) = A_R(x, y) \exp\{i[\varphi_R(x, y) + \Delta\varphi]\}. \quad (2)$$

The intensity profile of the interference pattern recorded by the image sensor is then given by

$$\begin{aligned} I_{\Delta\varphi}(x, y) &= |O(x, y, 0) + R_{\Delta\varphi}(x, y, 0)|^2 \\ &= A_O^2(x, y) + A_R^2(x, y) + 2A_O(x, y)A_R(x, y) \\ &\quad \times \cos[\varphi_O(x, y) - \varphi_R(x, y) - \Delta\varphi]. \end{aligned} \quad (3)$$

In the presented experiment, the reference beam is actually a plane wave which is normally incident onto the image sensor. Consequently, its amplitude  $A_R(x, y)$  and phase  $\varphi_R(x, y)$  are constant over the sensor and can be replaced by 1 and 0, respectively. From (3), it is straightforward to show that the complex object field at the output plane can be evaluated by combining the four intensity patterns resulting from the interference of the object beam with the reference

beam phase-shifted by the different values of  $\Delta\varphi$ . In this way, we are able to measure the phase

$$\varphi_O(x, y) = \arctan \left[ \frac{I_{\frac{\pi}{2}}(x, y) - I_{\frac{3\pi}{2}}(x, y)}{I_0(x, y) - I_{\pi}(x, y)} \right] \quad (4)$$

and the amplitude

$$A_O(x, y) = \frac{1}{4} \sqrt{[I_0(x, y) - I_{\pi}(x, y)]^2 + [I_{\frac{\pi}{2}}(x, y) - I_{\frac{3\pi}{2}}(x, y)]^2}. \quad (5)$$

It will be shown in Section III that from these measurements of the amplitude and phase associated with the object wave in the sensor plane, it is possible to reconstruct the complex amplitude distribution,  $O(x', y', d)$ , generated by the 3-D object at different planes. This reconstruction can be done either optically or digitally.

### III. 3-D RECONSTRUCTION AND DISPLAY

#### A. Digital Reconstruction

In Section II, a way to measure the amplitude  $A_O(x, y)$  and phase  $\varphi_O(x, y)$  associated to the diffraction pattern of a 3-D object by phase-shift interferometry has been shown (see Fig. 1). The resulting complex digital hologram,  $O(x, y, 0)$  allows one to reconstruct numerically the complex amplitude distribution,  $O(x', y', d)$ , generated by the 3-D object at plane located at a distance  $d$  from the image sensor. The reconstruction process consists of simulating the propagation of the light. It can be obtained by computing the following discrete Fresnel integral:

$$\begin{aligned} O(m' \Delta x', n' \Delta y'; d) &= \exp \left[ -\frac{i\pi}{\lambda d} (m'^2 \Delta x'^2 + n'^2 \Delta y'^2) \right] \\ &\times \sum_{m=0}^{N_x-1} \sum_{n=0}^{N_y-1} O(m \Delta x, n \Delta y, 0) \\ &\times \exp \left[ -\frac{i\pi}{\lambda d} (m^2 \Delta x^2 + n^2 \Delta y^2) \right] \\ &\times \exp \left[ -i2\pi \left( \frac{m'm}{N_x} + \frac{n'n}{N_y} \right) \right] \end{aligned} \quad (6)$$

where the spatial resolutions at the CCD plane and at the object planes are denoted by  $(\Delta x, \Delta y)$  and  $(\Delta x', \Delta y')$ , respectively.  $N_x$  and  $N_y$  are the number of samples in the  $x$  and  $y$  directions. The variables  $(m, n)$  and  $(m', n')$  are discrete spatial coordinates in the CCD plane and the object plane, respectively. Equation (6) can be computed using a fast Fourier transform algorithm. It can be shown that the resolutions  $\Delta x'$  and  $\Delta y'$  along the horizontal and vertical transversal directions at the object space are given by

$$\Delta x' = \frac{\lambda d}{N_x \Delta x}, \quad \text{and} \quad \Delta y' = \frac{\lambda d}{N_y \Delta y}. \quad (7)$$

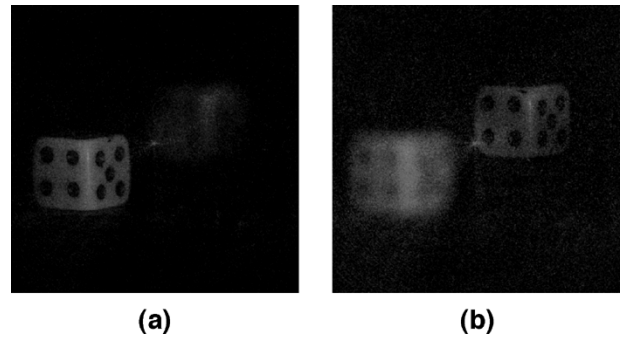


**Fig. 2.** Gray-level picture of the irradiance distribution reconstructed from a single digital hologram at two distances. (a)  $d = 315$  mm. (b)  $d = 345$  mm.

Therefore, in the reconstruction of a view of the 3-D input object with (6), the transversal resolution  $(\Delta x', \Delta y')$  changes with the value of the distance  $d$ .

An alternative way to reconstruct the complex amplitude distribution  $O(x', y', d)$  is to use the propagation transfer function method instead of (6), i.e.,

$$\begin{aligned} O(m' \Delta x', n' \Delta y'; d) &= F^{-1} \left\{ F [O(m \Delta x, n \Delta y, 0)] \right. \\ &\times \exp \left[ -i\pi \lambda d \left( \frac{u^2}{(\Delta x N_x)^2} + \frac{v^2}{(\Delta y N_y)^2} \right) \right] \left. \right\} \end{aligned} \quad (8)$$

where  $F$  denotes the fast Fourier transform, and  $u$  and  $v$  are discrete spatial frequencies. In this approach, the resolution at the output plane is the same for any propagation distance  $d$  and is given by the resolution at the input plane, i.e., the size of the pixels in the CCD sensor. The calculation method is selected by the propagation distance according to the satisfaction of the sampling theory. Another method to compute  $O(x', y', d)$  without using fast Fourier transforms is described in [40].

As an example, the irradiance distributions corresponding to two different reconstructions of the same digital hologram computed with (8) are shown in Fig. 2. The digital hologram was recorded with the optical setup in Fig. 1 by use of an argon laser with wavelength 514.5 nm. The detector was a CCD image sensor with  $(N_x, N_y) = (2048, 2048)$  pixels with size  $(\Delta x, \Delta y) = (9, 9) \mu\text{m}$ . The scene contains two cubic dice with a lateral size equal to 4.6 mm. Fig. 2(a) shows the irradiance at a distance  $d = 315$  mm, whereas Fig. 2(b) is that obtained for  $d = 345$  mm. From Fig. 2 it is clear that it is possible to reconstruct the input scene at different distances starting from the same digital hologram.

As in conventional holography, different regions of the digital hologram record light arising from different perspectives of the 3-D object. Thus, we can also reconstruct different views of the 3-D object by using partial windows of the digital hologram and applying (6) or (8). Of course, this method implies losing some information because we do not use the full digital hologram to reconstruct the object. Furthermore, (6) and (8) simulate a propagation along an axis normal to the hologram and, therefore, each window provides a different part of the object plane. This effect is shown in Fig. 3(a) for the

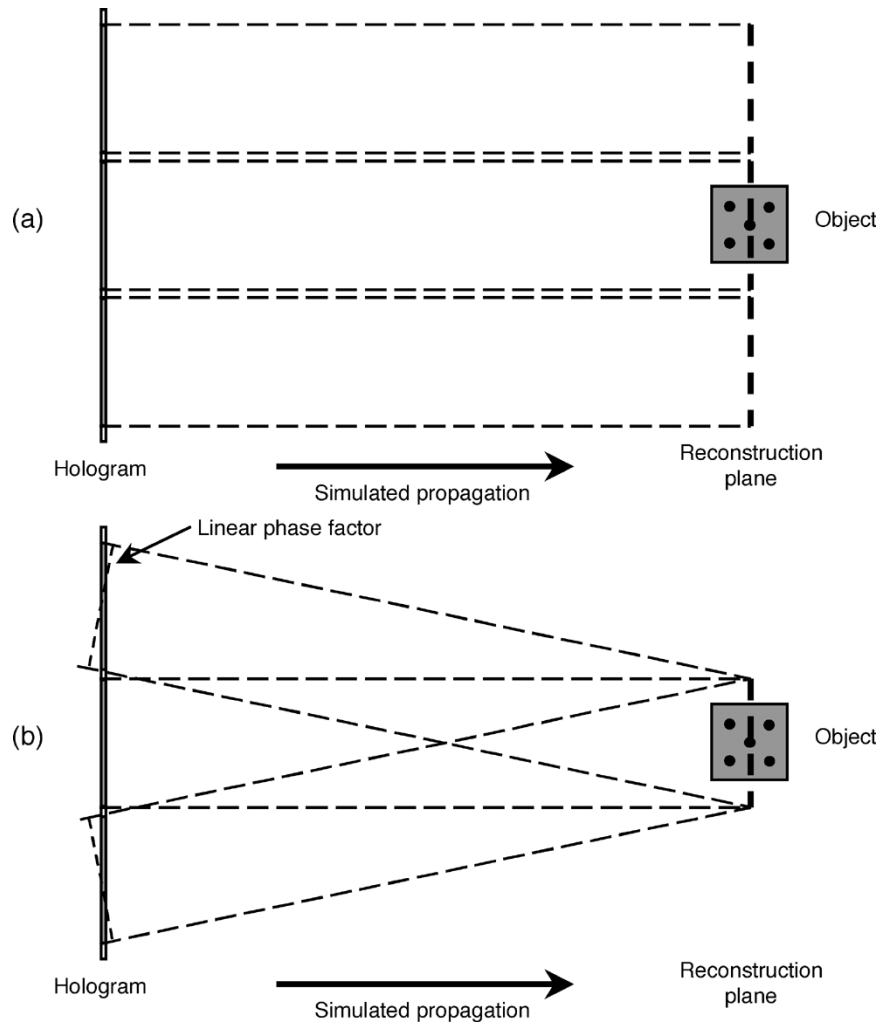


**Fig. 3.** Reconstruction of perspectives by using partial windows in the digital hologram. (a) Without phase factor. (b) With a linear phase factor to recenter the reconstruction view.

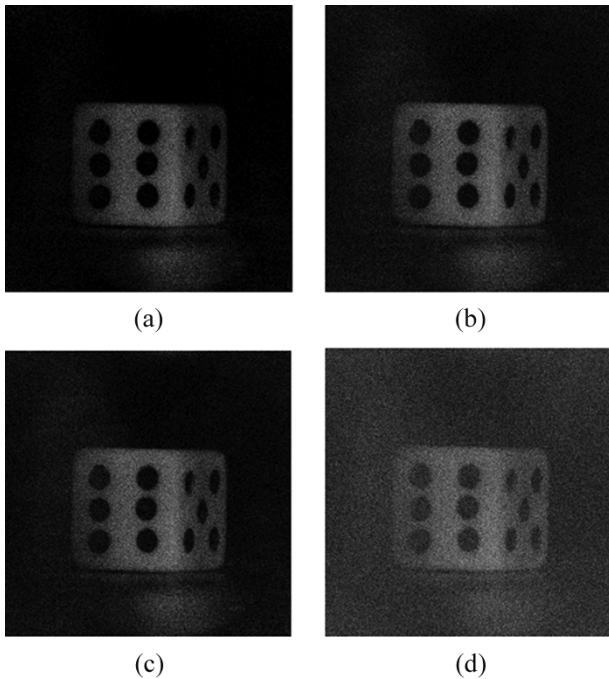


**Fig. 4.** Reconstructed images by use of: (a) complex field data and the phase-only data; (b) without the quantization; (c) and (d) with quantization reduction to 5 bits and 1 bit, respectively.

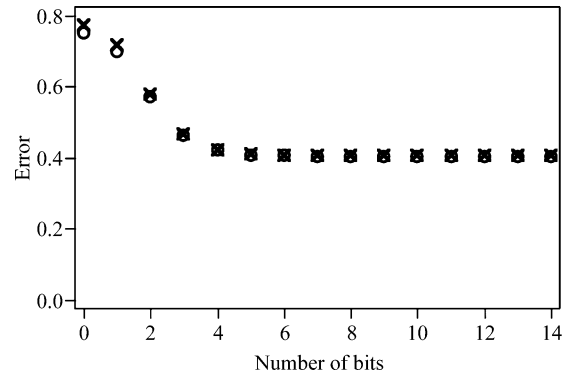


**Fig. 5.** Error as a function of a number of phase levels with different images (O and X).

case of (8). In order to reconstruct perspectives centered at the same point, we need to multiply each window by a linear phase factor, which is equivalent to considering a tilted plane wave illuminating the digital hologram (see Fig. 3(b)). In mathematical terms, in (6) or (8) we need to replace  $O(m\Delta x, n\Delta y, 0)$  with  $W_{ab}(m\Delta x, n\Delta y) \exp[-i2\pi(a m\Delta x + b n\Delta y)/\lambda d]$ , where  $W_{ab}(m\Delta x, n\Delta y)$  is the window centered at coordinates  $(a, b)$  in the hologram. The angle of view with respect to the orthogonal axis is then  $(\alpha, \beta) = (a/d, b/d)$ . Note that

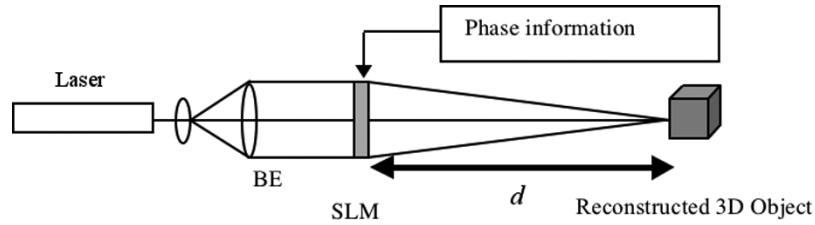


Fig. 6. Optical reconstruction system. BE: beam expander; SLM: spatial light modulator.

the maximum angle of reconstruction is limited only by the size of the detector.

The reconstruction of a 3-D object can also be performed by discarding the amplitude information  $A_O(x, y)$  of the hologram and using its sole phase information  $\varphi_O(x, y)$ . Fig. 4(a) and (b) show an example of the reconstructed images of a die by use of the fully complex field and phase-only information, respectively. We also reconstruct the object by use of the phase distribution with quantization reductions to 5 bits and 1 bit as shown in Fig. 4(c) and (d). As can be seen in Fig. 4, as little as a 5-bit representation of the phase distribution can reconstruct the object with moderate error. This error between the reconstructed 3-D object from the complex field and phase-only field is evaluated using the following criterion:

$$E = \sum_{m'=1}^{N_y} \sum_{n'=1}^{N_y} \left( |O(m' \Delta x', n' \Delta y'; d)|^2 - \left| \hat{O}(m' \Delta x', n' \Delta y'; d) \right|^2 \right)^2 \quad (9)$$

where  $|O(m' \Delta x', n' \Delta y'; d)|^2$  and  $|\hat{O}(m' \Delta x', n' \Delta y'; d)|^2$  are the reconstructed intensity images at propagation distance  $d$  by use of fully complex field and phase-only field, respectively. The power in each of these images is normalized. Fig. 5 shows the error as a function of the number of bits used to quantize the phase-only information for two different images. The irreducible error obtained for high numbers of phase levels is caused by the elimination of the amplitude information. Although the quantitative error in Fig. 5 is high, it can be seen in Fig. 4 that the object is properly reconstructed. This means that the error reported by Fig. 5 is mainly due to the incorrect reconstruction of the speckle pattern.

### B. Optical Reconstruction

As shown in Section III-A, a 3-D object can be reconstructed numerically by simulating the Fresnel diffraction. However, this calculation is computationally intensive. It requires several tens of seconds on a personal computer for a  $2048 \times 2048$  pixel hologram, making it difficult to construct a real-time display. It is possible to use an optical reconstruction system for real-time display of 3-D objects [28]. As shown in the previous section, the reconstruction can be performed by use of the sole phase information  $\varphi_O(x, y)$  of the hologram. This phase-only information is easier to display on commercially available liquid crystal spatial light modulators (SLMs) than the full complex field.

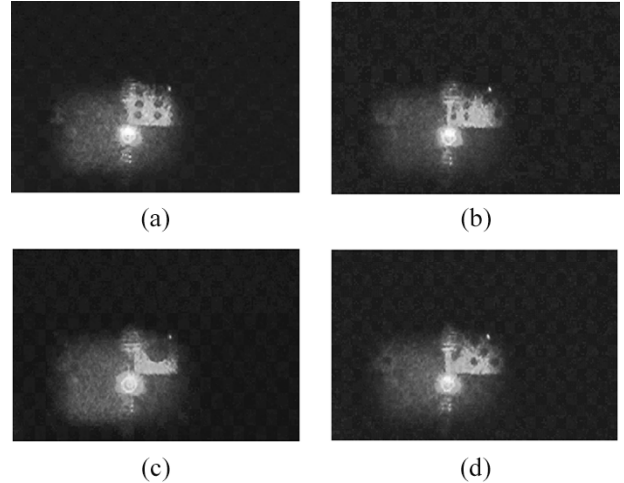


Fig. 7. Optically reconstructed images.

Moreover, in a practical system, there is a limit on the number of phase levels that can be displayed on a phase-only SLM. The previous section demonstrated that a small number of phase levels permits a satisfactory reconstruction, which indicates that commercially available SLMs can be used for the optical reconstruction by phase-only information.

To demonstrate a real-time 3-D display, several holograms of a die are recorded using a four-step phase-shift interferometer similar to the one used in Fig. 1. The die is mounted on a rotary stage controlled by a personal computer. For each rotation of the die—in  $15^\circ$  steps—four interference patterns are recorded and used to compute the digital hologram as explained in Section II. The optical reconstruction of the 3-D die is then implemented using the optical setup shown in Fig. 6. After collimation and expansion, the laser beam illuminates a liquid crystal SLM with  $1024 \times 768$  pixels on which is displayed the phase-only information from the digital holograms. Fig. 7 shows optically reconstructed images. The quality of the images is not as good as with the numerical reconstruction because the SLM has a nonlinear phase retardation response and does not permit a full  $2\pi$  phase modulation [28]. However, this experiment demonstrates that a real or a virtual 3-D object can be reconstructed in real-time by use of phase-only information.

### IV. 3-D OBJECT COMPRESSION

A single  $2028 \times 2044$  pixel digital hologram requires 65 MB of storage in its native double precision format (8 B of amplitude information and 8 B of phase information in each pixel). For more efficient storage and transmission, it would be very useful to compress these digital holograms.

**Table 1**  
Lossless Compression of Digital Holograms (Compressed as Separate Real and Imaginary Data Streams)

Hol. no.	Size (kB)	Compression ratio							
		LZ77 (kB)	LZW (kB)	Huff. (kB)	BW (kB)	LZ77	LZW	Huff.	BW
1	64,769	9356+9127	8931+8791	13,899+13,079	6389+6263	3.50	3.65	2.40	5.12
2	64,769	29,890+29,752	32,385+32,385	30,987+31,009	24,413+24,163	1.09	1.00	1.04	1.33
3	64,642	7254+8180	7747+8318	27,154+27,282	4512+5199	4.19	4.02	1.19	6.66
4	64,769	9465+9125	9047+8805	13,815+13,027	6512+6283	3.48	3.63	2.41	5.06
5	64,769	9227+9061	8839+8718	13,439+13,082	6336+6265	3.54	3.69	2.44	5.14
Averages:						3.16	3.20	1.90	4.66

Compression of digital holograms differs to image compression principally because digital holograms store 3-D information in complex-valued pixels, and second because of the speckle content which gives them a white-noise appearance.

### A. Lossless Compression

A first approach consists of applying to digital holograms various classical lossless compression algorithms such as Huffman coding [41], Lempel–Ziv coding [42] (LZ77), Lempel–Ziv–Welch coding [43] (LZW), and Burrows–Wheeler coding [44] (BW). Table 1 contains the results of applying these techniques to five digital holograms. Compression ratio  $r$  is defined as

$$r = \frac{\text{uncompressed size}}{\text{compressed size}}. \quad (10)$$

Each digital hologram was represented as two separate real and imaginary binary data streams. This admitted better compression than a pixel-wise representation (alternating real and imaginary values) and than amplitude and phase representations. As shown in Table 1, on average, each bit of compressed data encodes 4.66 bits of uncompressed holographic data (with BW), and the real and imaginary streams are equally difficult to compress. Given their size, it is of concern how poorly these techniques perform, and how some holograms (no. 2, for example) almost completely resist lossless compression. These poor results can be explained by the noise-like aspect of the digital holograms. The speckle pattern is due to spatially random interferences inherent to the diffusion on rough objects; it can be reduced but not removed completely. This motivates the need for lossy compression.

### B. Quantization of Digital Holographic Data

It was already shown in Section III-A that it is possible to discard the amplitude information of the holograms and apply some quantization on the remaining phase information. Other treatments of quantization in holograms can be found in the literature [29], [30], [45], [46].

Note that the effect of the loss of information due to quantization is of no interest in the decompressed hologram itself, but rather in the subsequent object reconstruction. In a way similar to (9), a reconstructed-object-plane normalized

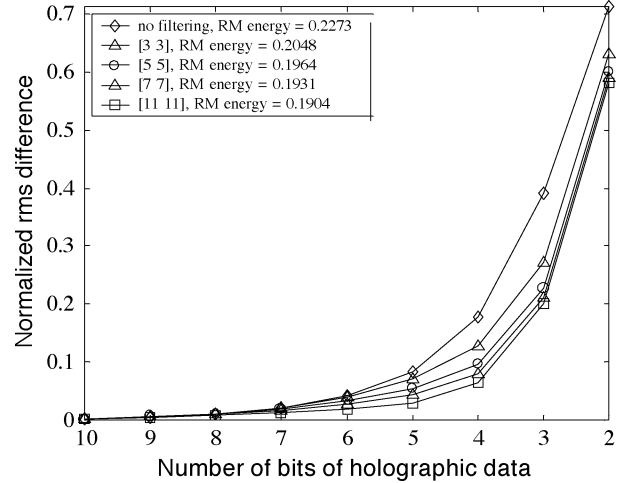


**Fig. 8.** Error plotted against number of bits in each of the real and imaginary values for hologram no. 1.

rms metric can be defined to quantify the quality of the lossy compressed holograms

$$E = \sum_{m'=1}^{N_y} \sum_{n'=1}^{N_y} \left( |O(m' \Delta x', n' \Delta y'; d)|^2 - |\hat{O}(m' \Delta x', n' \Delta y'; d)|^2 \right)^2 \quad (11)$$

where  $|O(m' \Delta x', n' \Delta y'; d)|^2$  and  $|\hat{O}(m' \Delta x', n' \Delta y'; d)|^2$  are now the reconstructed intensity images at propagation distance  $d$  by use of the original and the decompressed hologram, respectively. The slightest change to a digital hologram can result in an entirely different speckle pattern in the reconstruction domain. In order to remove this somewhat quantization-invariant speckle effect before measuring the quantization error, a combination of mean filtering, median filtering, and subsampling in the reconstructed intensity field is used (see for instance [37]).

In order to optimize the use of the dynamic range, the holograms are linearly rescaled so that their real and imaginary components are comprised between  $[-1, 1]$  and  $[-i, i]$ , respectively. The real and imaginary components of each holographic pixel are then quantized. An odd number of quantization values (or levels) is chosen for each real and imaginary value: zero, and an equal number of positive and negative levels. As a result  $b$  bits encode  $(2^b - 1)$  levels. For example,

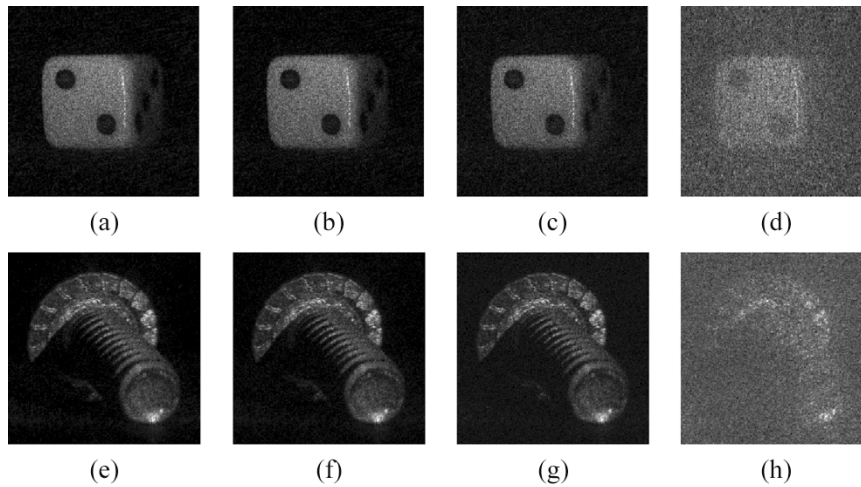


**Fig. 9.** Reconstructed views from quantized digital holograms with different numbers of bits of resolution in each real and imaginary value: (a)–(d) Hologram no. 1 with no quantization; 4, 3, and 2 bits, respectively. (e)–(h) Hologram no. 2 with no quantization; 4, 3, and 2 bits, respectively.

two bits encode levels  $\{-1, 0, 1\}$ , three bits encode levels  $\{-1, -2/3, -1/3, 0, 1/3, 2/3, 1\}$ , and so on.

Five different holograms are used in the quantization experiments. Fig. 8 shows a plot of error against number of bits per (real and imaginary) data value for hologram no. 1 for each of five median filtering neighborhoods from  $1 \times 1$  pixels (no filtering) to  $11 \times 11$  pixels. Each of the other four holograms had a similar response. Fig. 9 shows reconstructed object intensities for hologram nos. 1 and 2 for selected quantization resolutions and with  $4 \times 4$  subsampling (integrating each  $4 \times 4$  nonoverlapping block to a single value) to reduce noise. Quantization at 4 bits yields a good quality reconstruction and a normalized rms error of less than 0.1 (with filtering), and corresponds to a compression ratio of 16 (prior to the application of a lossless technique).

### C. Fourier-Domain Processing

The JPEG algorithm also performs most of its compression during a quantization stage. However, it uses the discrete cosine transform to allow it to perform quantization in the spatial frequency domain. The JPEG standard is defined for real-valued images only, but can be adapted to digital holograms, taking instead the discrete Fourier transform (DFT) of each nonoverlapping block of  $8 \times 8$  pixels. Rounding errors aside, this will not reduce the amount of information in the image but will tend to concentrate the majority of the hologram information into a few DFT coefficients in each block. A fixed number of the smallest DFT coefficients in each block is then set to zero. This involves sorting the values in each  $8 \times 8$  DFT and setting the  $(64 - n)$  lowest-valued coefficients to zero, where  $n \in [1, 64]$  denotes the number of DFT coefficients to be retained in each block. Sorting of the DFT coefficients is performed by amplitude first, and then (if necessary) by phase angle. Fig. 10 shows error for hologram no. 1 for selected values of  $n$ . The results are consistent over all holograms: with  $11 \times 11$  filtering, as many as 78% (50/64) of the DFT coefficients can be removed for normalized rms errors of less than 0.1, giving an initial compression ratio of 4.6 (64/14), which can be further improved

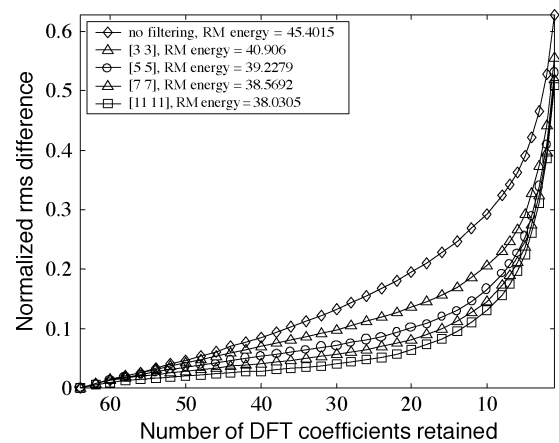


**Fig. 10.** Error against number of DFT coefficients retained, for hologram no. 1 for various median filter neighborhoods.

by applying quantization and lossless compression to the remaining Fourier components.

## V. 3-D OBJECT ENCRYPTION

Information security is a very important issue in data communication and storage. In a holographic system, encryption can be easily introduced by using random phase modulation, either in the reference or in the object beam [33]–[35]. In this section, we present three types of secure digital holograms. In all three cases, the original 3-D object can be reconstructed either optically—in real time—or digitally.

### A. Encryption of the Reference Beam

Fig. 11(a) shows one of the 3-D image encryption systems [33]. In this case, the reference beam is modulated by a random phase mask and then the encrypted holographic data is recorded by an image sensor. The encrypted complex field can be obtained using phase shifting digital holography. To decrypt the information, one has to measure the complex field of the random phase mask at the image sensor plane. Fig. 11(b) shows the measurement system of the complex field of the random phase mask. Fig. 12(a) shows the reconstructed image

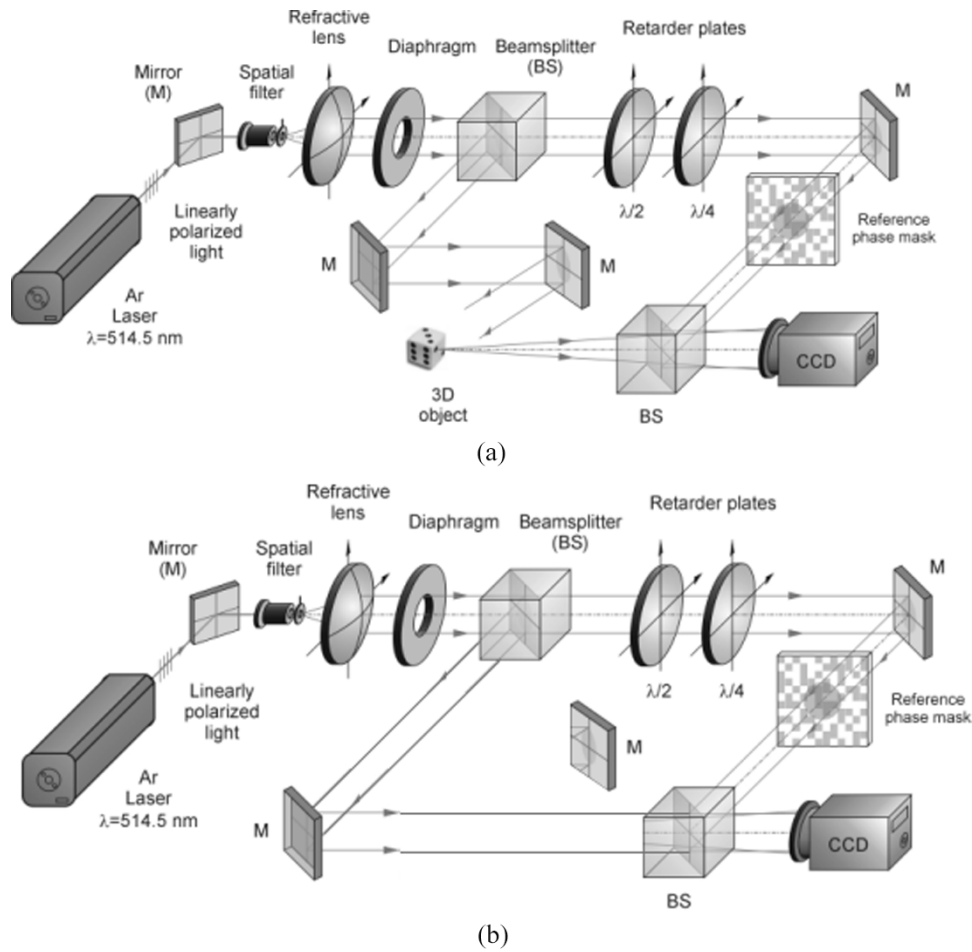


**Fig. 11.** Encrypted 3-D display system. (a) Recording an encrypted 3-D object. (b) Recording the information of the random phase mask.

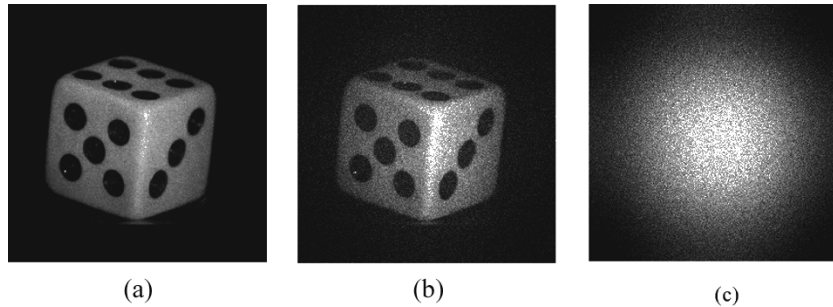


**Fig. 12.** Reconstructed images. (a) Without the encryption. (b) With the encryption and the correct phase information. (c) With the encryption and incorrect phase information.

of the input 3-D object without the random phase encryption that is obtained by phase shifting digital holography. By introducing the encryption technique in the reference arm, the reconstructed image is presented in Fig. 12(b). The quality of the reconstructed data is not as good as the original because of the loss of the scattered data and complex structures in the phase information. However, the reconstructed 3-D object still has good quality. When the incorrect key is used, the reconstructed data becomes white-noise-like data as shown in Fig. 12(c).

### B. Fourier Encryption of the Object Beam

Fig. 13 presents another type of 3-D image encryption system [34], [35]. In this system, 3-D object information itself is encrypted by a random phase mask located at the Fourier plane. Let  $p(x', y') = O(x', y'; d)$  be the complex field of the object in the object focal plane of the first lens. This function is the plain unencrypted data and contains the full 3-D information of the object. It is Fourier transformed by the first lens, then multiplied by a random phase mask in



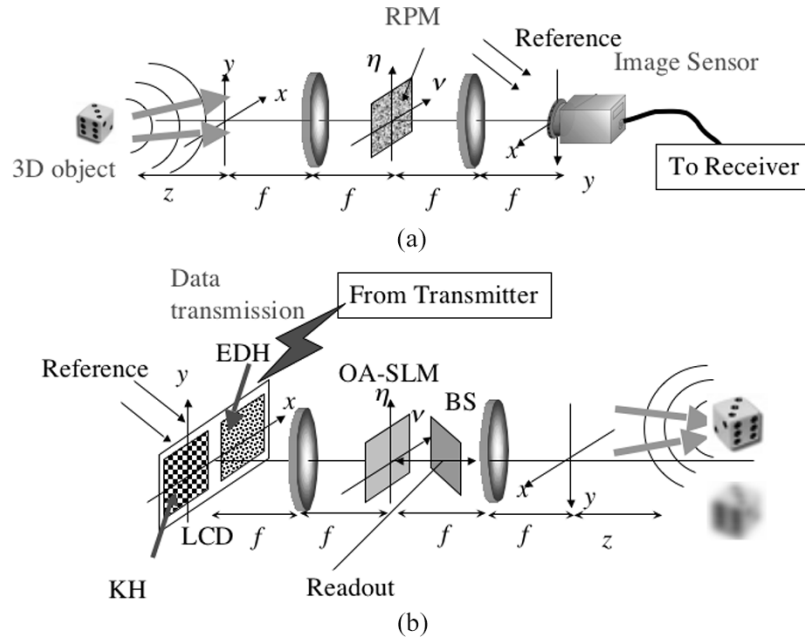


Fig. 13. Secure 3-D display system with object encryption: (a) recording and (b) reconstruction systems.

the Fourier plane as shown in Fig. 13(a). The resulting complex field is

$$E(\mu, \nu) = P(\mu, \nu)M(\mu, \nu) \quad (12)$$

where  $P(\mu, \nu)$  is the Fourier transform of  $p(x', y')$  and  $M(\mu, \nu)$  is the phase mask. Here  $\mu$  and  $\nu$  are the coordinates in the Fourier plane. After performing another Fourier transform with the second lens, the encrypted pattern at the image sensor plane is described by

$$e(x, y) = p(x, y) \otimes m(x, y) \quad (13)$$

where  $\otimes$  denotes convolution and  $m(x, y)$  is the Fourier transformed pattern of the random phase mask  $M(\mu, \nu)$ . This encrypted information is recorded as an encrypted digital hologram by making an interference pattern with a plane reference wave.

The key hologram is the interference pattern between only the random phase mask at the Fourier plane and the reference beam. This key hologram is sent to the authorized user in advance using a secure channel. Encrypted digital holograms can later be transmitted via an unsecure channel. In the reconstruction, both encrypted and key digital holograms are needed to decrypt the data and to reconstruct the 3-D object.

To decrypt the data, an optical joint transform correlator is used because the phase modulation was originally performed in the Fourier plane. Both the encrypted and key digital holograms are placed side-by-side in the input plane [Fig. 13(b)]. The encrypted digital hologram is shifted from the hologram key at a distance of  $\alpha$  along the  $x$  axis. The input image is illuminated by the plane reference beam that has the same characteristics (incident angle and wavelength) used in the

recording system. If the reference wave is tilted to spatially separate the diffracted light from the transmitted light, the following term can be isolated:

$$t(x', y') = e(x' - \alpha, y') + m(x', y'). \quad (14)$$

The diffracted light beam described in (14) is Fourier-transformed by a lens and then recorded as a joint power spectrum (JPS) in an intensity sensitive SLM such as an optically addressed spatial light modulator (OA-SLM). The JPS is described as

$$\begin{aligned} |T(\mu, \nu)|^2 &= |E(\mu, \nu) \exp\{i\alpha\mu\} + M(\mu, \nu)|^2 \\ &= |E(\mu, \nu)|^2 + |M(\mu, \nu)|^2 \\ &\quad + E(\mu, \nu) \exp\{i\alpha\mu\} M^*(\mu, \nu) \\ &\quad + E^*(\mu, \nu) \exp\{-i\alpha\mu\} M(\mu, \nu) \end{aligned} \quad (15)$$

where  $T(\mu, \nu)$  is the Fourier transform of  $t(x', y')$  and  $*$  denotes complex conjugate. Using (12) and considering that  $|M(\nu, \eta)| = 1$  because a phase-only mask is used, we get

$$\begin{aligned} |T(\mu, \nu)|^2 &= |E(\mu, \nu)|^2 + 1 + P(\mu, \nu)M(\mu, \nu) \\ &\quad \times \exp\{i\alpha\mu\} M^*(\mu, \nu) + P^*(\mu, \nu)M^*(\mu, \nu) \\ &\quad \times \exp\{-i\alpha\mu\} M(\mu, \nu) \\ &= |E(\mu, \nu)|^2 + 1 + P(\mu, \nu) \exp\{i\alpha\mu\} \\ &\quad + P^*(\mu, \nu) \exp\{-i\alpha\mu\}. \end{aligned} \quad (16)$$

By illuminating the OA-SLM with another plane wave for the readout and then Fourier-transforming (16) by a lens, we obtain the output signals

$$o(x, y) = e(x, y) \bullet e(x, y) + \delta(x, y) + p(x - \alpha) + p^*(x + \alpha) \quad (17)$$

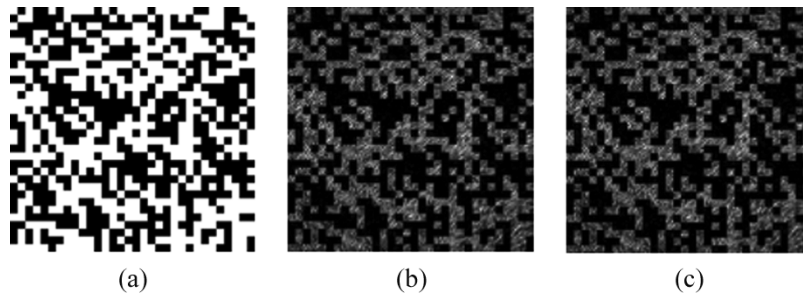


**Fig. 14.** Numerical results. (a) Input data. (b) Reconstructed data without quantization. (c) Reconstructed data with quantization reduction to 8 bits.

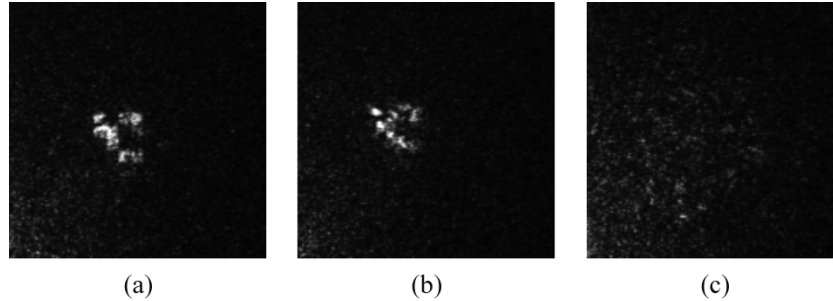


**Fig. 15.** Reconstructed images: (a) at the correct position and (b) at incorrect position when the correct key hologram is used. (c) Reconstructed image at correct position when the incorrect key hologram is used.

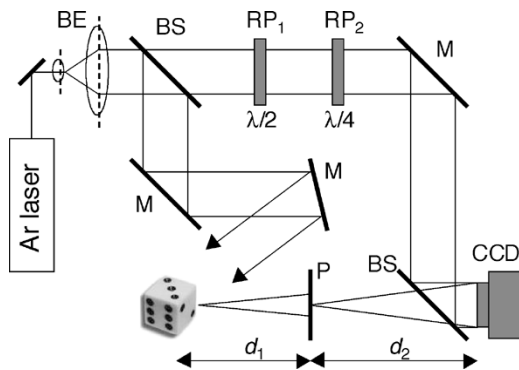


**Fig. 16.** Experimental setup for 3-D object encryption using phase-shift digital holography. BE: beam expander; BS: beam splitter; M: mirror; RP: retardation plate; P: phase mask.

where  $\bullet$  denotes correlation. The third term of (17) shows that—if the spatial separation between the autocorrelations and the reconstructed objects is sufficient—the original 3-D object can be successfully reconstructed.

Fig. 14 presents a numerical simulation of a decrypted two-dimensional image. In the construction of the optical system, a critical device is the OA-SLM that records the JPS. An important factor is the intensity levels that can be recorded. Fig. 14 shows that a JPS quantization reduction to 8 bits gives almost as good results as the case of no quantization. However, it can be shown that a JPS quantization reduction to 6 bits cannot reconstruct the original data.

The next step is to demonstrate an optical decryption. Unfortunately, the spatial and intensity resolution of currently available OA-SLMs is not sufficient to satisfactorily record the JPS. We therefore present the optical reconstruction of a digitally computed JPS. The JPS is displayed on a  $1024 \times$

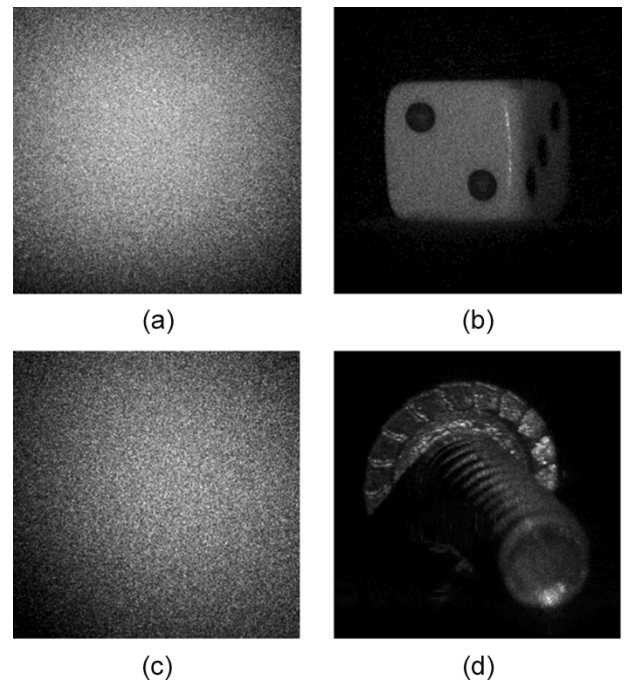


**Fig. 17.** Reconstruction of the die hologram: (a) without the phase mask, and (b) with the phase mask; reconstruction of the bolt hologram: (c) without the phase mask, and (d) with the phase mask.

768 pixel liquid-crystal SLM with 256 levels of amplitude modulation. The reconstructed images are shown in Fig. 15. When the correct key hologram is used, the original image is retrieved at the correct position as shown in Fig. 15(a). To show that the original image has 3-D information, the reconstructed image at an incorrect  $z$  position is shown in Fig. 15(b). The image then appears out of focus. When an

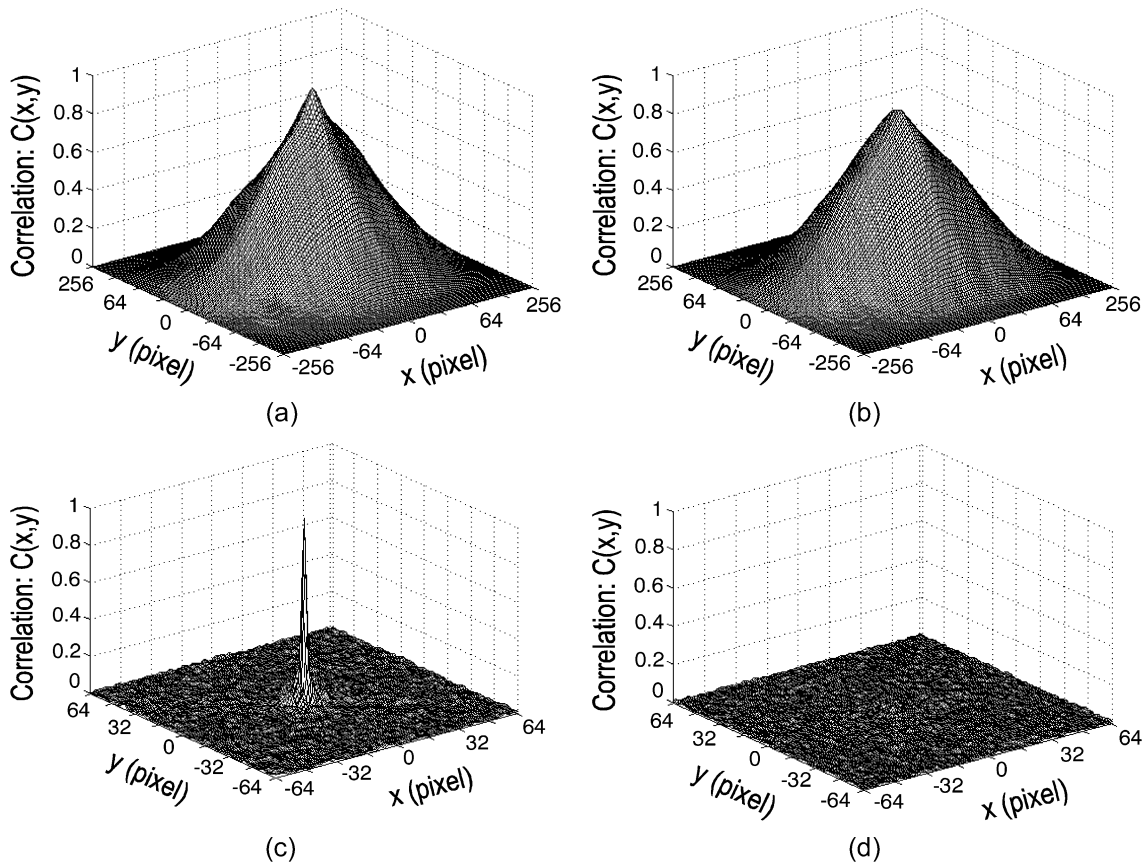


**Fig. 18.** Comparison between two different model cars. (a) Conventional autocorrelation and (b) conventional cross correlation between their 2-D intensity images. (c) 3-D autocorrelation and (d) 3-D cross correlation of their digital holograms.

incorrect key hologram is used, the reconstructed image is still a white-noise-like image as shown in Fig. 15(c).

### C. Fresnel Encryption of the Object Beam

Another encryption technique consists of placing a random phase mask in the Fresnel field, between the object and the sensor (Fig. 16). Let  $p(x', y') = O(x', y'; d)$  be the complex field of the object in plane P, just before the random phase mask. Again, this function—that contains the full 3-D information of the object—is the original unencrypted data. After the phase mask, the complex field is simply

$$p(x', y') \exp[i\phi_M(x', y')] \quad (18)$$

with  $\phi_M(x', y')$  the phase of the mask. By free-space propagation [47], the encrypted light field in the camera plane is then given by

$$e(x', y') = \{p(x', y') \exp[i\phi_M(x', y')]\} \otimes g_{d_2}(x', y') \quad (19)$$

where  $\otimes$  stands for convolution and the free-space propagation kernel is

$$g_{d_2}(x', y') = \exp\left\{\frac{i\pi}{\lambda d_2} (x'^2 + y'^2)\right\}. \quad (20)$$

Due to free-space propagation, the signal at the detector plane has both its amplitude and phase modulated by the mask and has a dynamic range suitable for capture by a CCD camera. Both the amplitude and the phase look like random noise distributions. The phase-shift digital holography procedure allows the full encrypted wavefront to be captured. In this system, the encryption key consists of the random phase mask, its position in 3-D space, the wavelength of the illumination, the dimensions of the detector elements (for a pixelated device), and the distance between the mask and the notional center of the object.

Now, the decryption and reconstruction of the digital hologram is a two-stage process. Each stage could be performed optically or digitally. First, the hologram is propagated a distance  $d_2$  to plane P. Second, the hologram is decrypted by multiplication with the phase mask and is reconstructed through further Fresnel propagation to focus in any chosen object plane.

Note that this encryption method can be performed optically or digitally (in software). In particular, unencrypted digital holograms can be retrospectively encrypted digitally such that they are in a suitable form for optical decryption and reconstruction. Note also that once the encrypted wavefront is known in digital form, it is easy to compute its complex conjugate, which avoids the need for time-reversed Fresnel reconstruction expressions and permits the use of the exact same phase mask (rather than its conjugate) in any optical reconstruction.

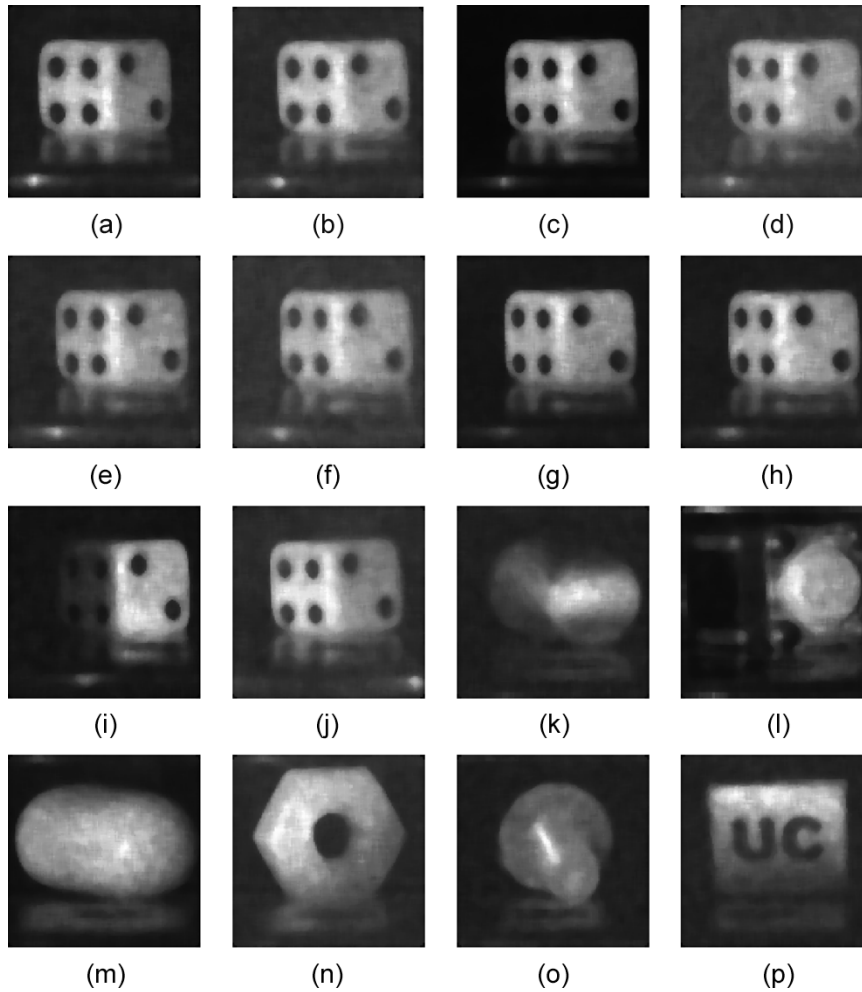


**Fig. 19.** Images reconstructed from digital holograms used for rotation-tolerant 3-D pattern recognition. (a)–(h) Examples of views of the reference die with various orientations. (i) Reference die with a different illumination. (j) Laterally and longitudinally shifted reference die. The image is reconstructed in the new location of the object. (k)–(p) False targets.

In the experiments presented in [30], holograms that were initially captured without a random phase mask were retrospectively encrypted. By digitally simulating the encryption procedure, flexibility and security is gained, while still accommodating the possibility for a real-time optical reconstruction (see Section III-B). The phase mask used in the experiments consists of values chosen with uniform probability from the range  $[0, 2\pi)$  using a pseudorandom number generator. The mask has dimensions  $2048 \times 2048$  pixels and is positioned as shown in Fig. 16 such that the ratio of the distances  $d_1 : d_2$  is 35 : 65. In Fig. 17, the results of reconstructing an encrypted digital hologram with and without the phase mask used in the encryption step are shown.

## VI. 3-D OBJECT RECOGNITION

### A. 3-D Recognition Using Phase-Shift Digital Holography

The 3-D information contained in a phase-shift digital hologram can be utilized to perform recognition of 3-D objects. The simplest way of comparing two 3-D objects is to directly perform a correlation between their respective digital holograms [36]. An example of this technique is

presented in Fig. 18. This figure corresponds to an experiment in which digital holograms of two different model cars were recorded. Fig. 18(a) and 18(b), respectively, show the autocorrelation of one car and the cross correlation between both cars using a traditional 2-D correlation between intensity images of the cars. Fig. 18(c) and 18(d), respectively, show the same auto- and cross correlations using the 3-D correlation between the digital holograms. In the 3-D case, one observes both a strong narrowing of the autocorrelation peak and a dramatically increased discrimination in the cross correlation. These enhancements are permitted by the high spatial frequency speckle pattern that makes the correlations between holograms very sensitive to displacements of the objects. It is therefore possible to detect very small changes in the location or in the shape of an object. In addition, windows of the holograms can be used in the correlation instead of the full holograms (see Section III-A). By selecting different windows, it is possible to compare different perspectives of the objects and therefore to evaluate small rotations of the objects [36].

Because of its extreme sensitivity, the previous technique can only recognize an object almost perfectly similar to the

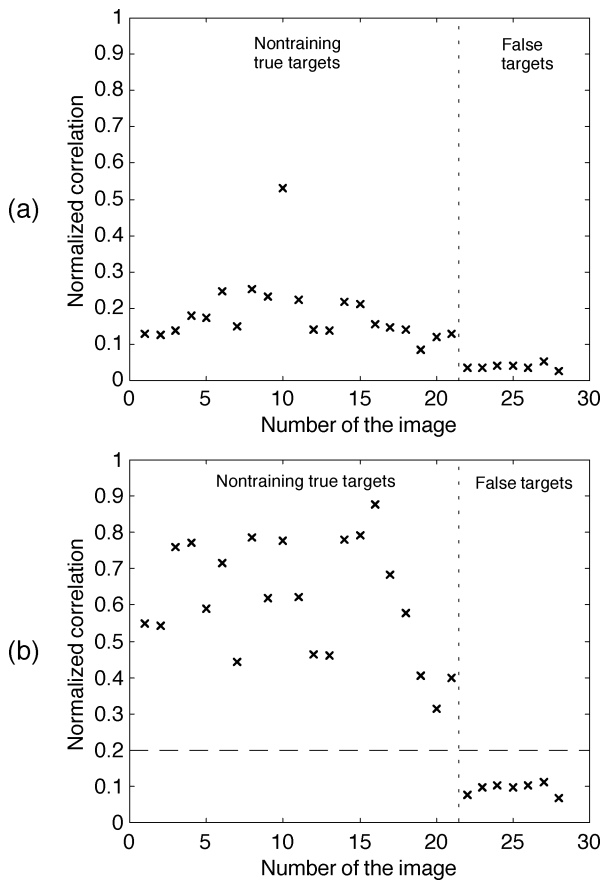


**Fig. 20.** Correlation peaks when comparing images reconstructed from digital holograms of various objects. Images #1–#21 correspond to the reference object with different orientations. Images #22–#28 are from other objects. (a) Filter made from one single view similar to Image #10. (b) Composite filter made from nine views based on three different holograms.

reference in shape, location and orientation. For many applications, a more robust technique is needed. It is possible to compute 3-D correlations on diffraction volumes computed from the holograms rather than on the holograms themselves. A diffraction volume is obtained by reconstructing the intensity distribution of the object beam in several planes of the object space [27]. The 3-D recognition is performed by computing the 3-D correlation between two reconstructed volumes. This technique features full 3-D shift invariance and is able to detect and locate an object in a 3-D scene. In practice, it is often possible to use a single 2-D reconstruction of the object as a reference, instead of the full reconstructed volume [27].

As mentioned above, various perspectives of an object can be reconstructed from different windows extracted from a digital hologram. However, the angle of view permitted by this method is very small, typically less than  $1^\circ$ . A way to recognize objects with larger rotations is to use composite correlation filters constructed with several rotated views of the 3-D reference object [48]. As an illustration, 19 holograms of a reference die are captured with different orientations of the die covering a  $9^\circ$  out-of-plane rotation range. One image of the die is reconstructed from each of these holograms (images #1–19). Fig. 19(a)–(h) present some of these images. Fig. 19(i) and 19(j) show images reconstructed from holograms of the same die in a different condition of

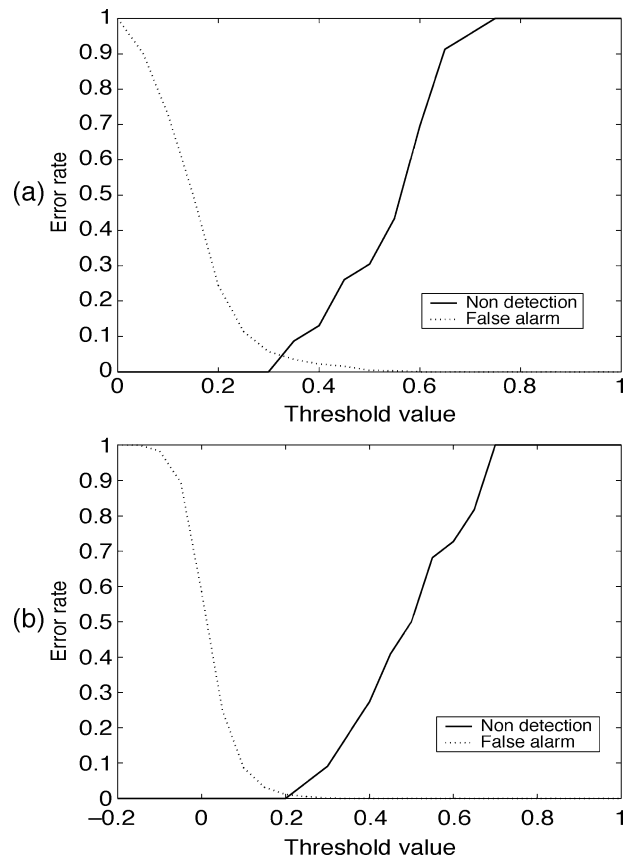


**Fig. 21.** Error rates for the recognition and orientation estimation of a die with a  $360^\circ$  rotation. (a) Using a bank of composite filters. (b) Using a bank of filters and a neural network.

illumination (image #20) and with a 85-mm displacement along the  $z$  axis (image #21), respectively. Images #1–21 all correspond to the reference die; they are the true targets. In Fig. 19(k)–(p) are shown images reconstructed from holograms of six different objects; these images (images #22–27), along with an image without any object (image #28), are the false targets. A correlation filter is first generated using a single view of the reference die. This view is reconstructed from the same hologram used for image #10, but with a different window. A nonlinear correlation is used in order to increase the discrimination capability [49]. Fig. 20(a) presents the correlation peak values for all images #1–28. Except for the one that is very similar to the training image, the true targets are barely distinguishable from the false targets. The rotation tolerance can be increased by constructing a composite filter with nine views of the die [37]. These views are obtained from three different holograms (corresponding to images #3, #10, and #16), using three windows in each hologram. Fig. 20(b) shows the correlation results. It is now possible to discriminate between (rotated) true targets and false targets using a threshold.

The rotation tolerance provided by the composite filter technique is limited to a few degrees. A way to deal with a  $360^\circ$  rotation range is to construct a bank of composite filters. Each filter is tuned to recognize a different range of rotations. The rotation of the object can then be determined by knowing which filter of the bank is fired up. As an example,

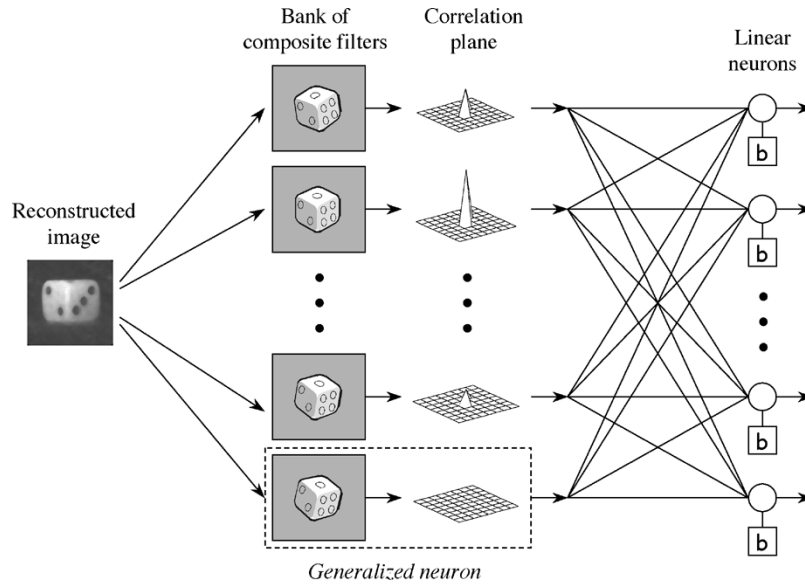


**Fig. 22.** Combination of a filter bank and a neural network for recognition and orientation estimation of a die.  $b$  denotes bias.

36 digital holograms of the previous die are recorded with a  $10^\circ$  rotation step. From these holograms, 36 rotation-tolerant composite filters are synthesized as described above. Since the recognition range of each filter is about  $10^\circ$ , the bank of filters now covers a  $360^\circ$  rotation range. However, it is difficult to determine the orientation of the die because of the self-similarity of its shape after rotations of  $90^\circ$ . As a test, 20 holograms of the die with various orientations and seven false targets are used. Fig. 21(a) presents the recognition error rates (nondetections and false alarms) versus the threshold applied to all the filters. The minimum error rate is around 5%. In order to improve the classification, the output of the filter bank is fed to a neural network composed of 36 linear neurons (Fig. 22). Each neuron responds to a particular orientation of the die, in  $10^\circ$  steps. The desired outputs are one for the neuron corresponding to the correct orientation and zero for the other neurons. The neuron weights are determined using 144 training images with known orientations. The training images are views of the die reconstructed from the same 36 holograms used for making the composite filters, but with different windows. Once the network is trained, its classification error rates are determined with the same 27 reconstructed images used for testing the sole filter layer. Fig. 21(b) shows that the minimum error is now reduced to less than 1%. The system is thus able to recognize and find the orientation of the die with any rotation angle.

### B. 3-D Recognition Using One-Shot On-Axis Digital Holography

As described above, phase-shift on axis digital holography requires the recording of multiple holograms. In contrast, one-shot on axis digital holography requires only a single digital hologram to recognize 3-D objects [50], [51]. The 3-D recognition can then be performed in real time. Additionally, the benefits of the proposed 3-D recognition method are greater simplicity and robustness to external

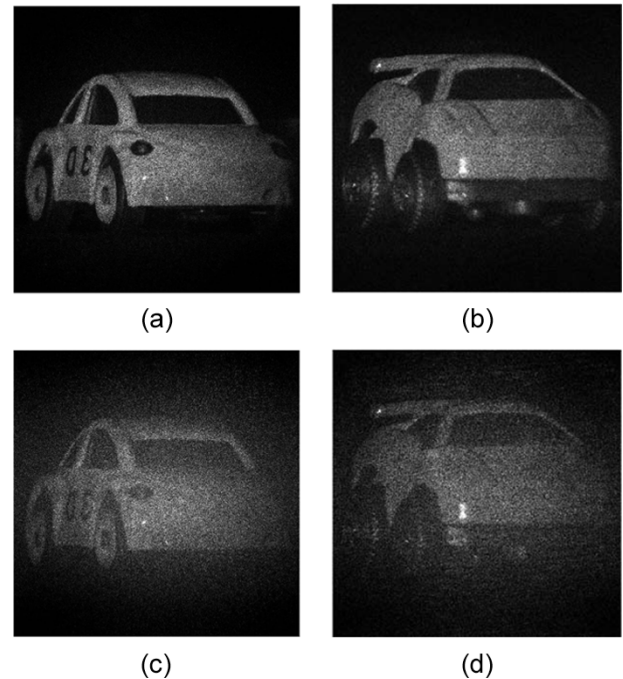


**Fig. 23.** (a) and (b) Images reconstructed by using conventional phase-shift digital holography: (a) car I and (b) car II. (c) and (d) are images reconstructed by using on axis one-shot digital holography with only a single hologram recording: (c) car I and (d) car II.

scene parameters such as moving targets and moving biological samples. This section experimentally shows that one-shot on axis digital holography is capable of providing 3-D object recognition.

For the on axis scheme, the unwanted zero order and conjugate object image terms are superimposed upon the reconstructed object image [24]. In phase-shift digital holography, these unwanted terms are eliminated through acquisition of multiple sequential holograms with known phase variations in the reference wave. This scheme requires a high stability in time of the optical setup. This shortcoming on 3-D object recognition by use of conventional digital holography

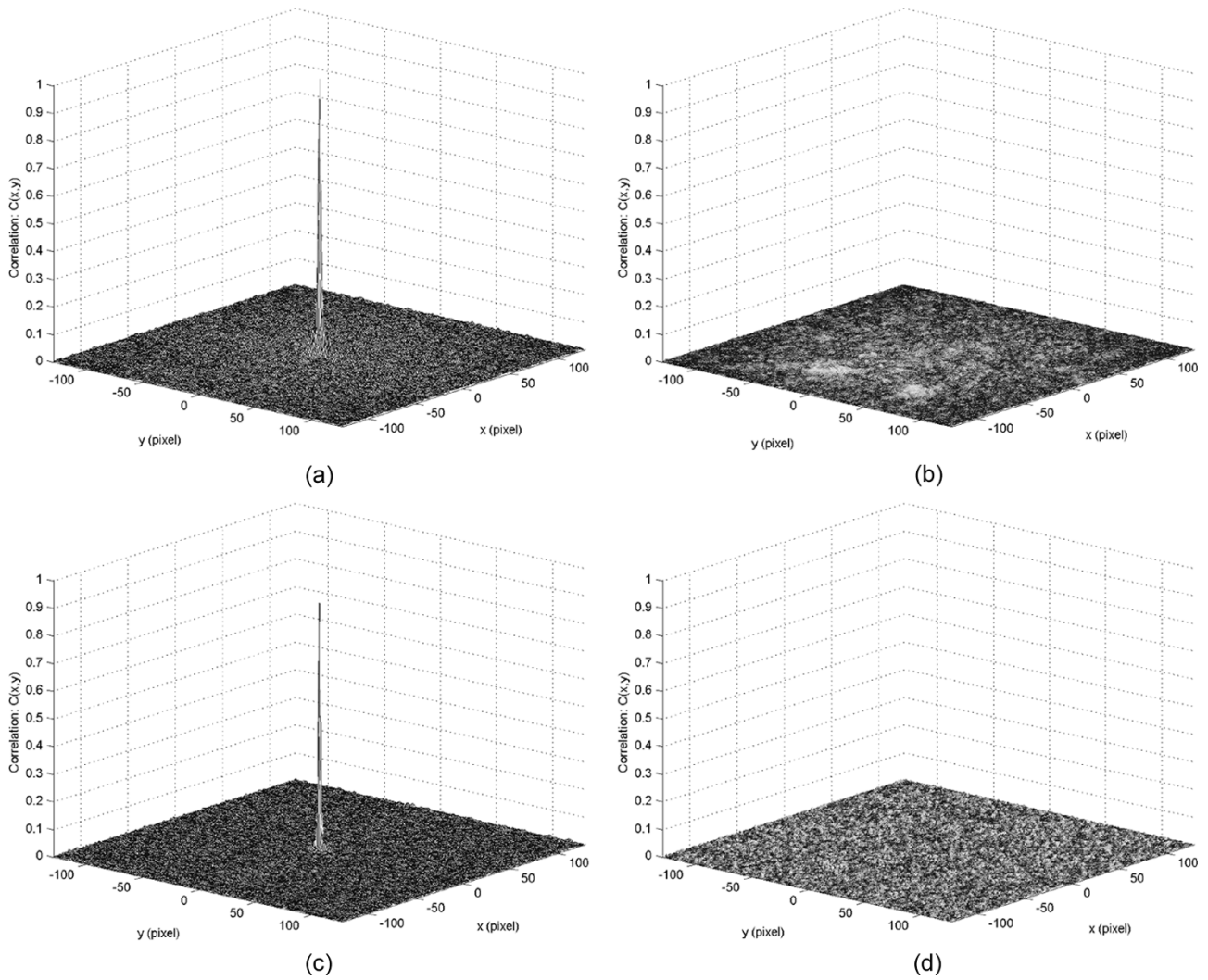


**Fig. 24.** (a) and (b) Autocorrelation and cross correlation of the holograms of car I and car II obtained by on axis phase-shift digital holography. (c) and (d) Autocorrelation and cross correlation of the holograms of car I and car II obtained by on axis one-shot digital holography.

can be overcome by using a one-shot scheme. In the on axis one-shot technique, the dc terms can be removed by spatially averaging the hologram. However, this technique still suffers from the conjugate image that degrades the reconstructed image quality. Fortunately for 3-D object recognition, the inherent conjugate term also contains information about the 3-D object and therefore does not substantially degrade the recognition.

As for phase-shift digital holography, the optical setup for the on axis one-shot digital holographic system is based on a Mach-Zehnder interferometer. In contrast to the conventional phase-shift scheme, no phase shifting components such as PZT actuator or phase retarders are required. In order to compare the 3-D object recognition capability of the on axis one-shot digital holographic technique with conventional on axis phase-shift method, experiments are conducted with two 3-D car objects as shown in Fig. 23. First, a hologram of 3-D car I is recorded. It corresponds to the reference object hologram which is used for generating a matched filter. The input target object (car I or car II) is then located at the distance  $d$  from the CCD camera. A numerically reconstructed complex wave for car I and

car II can be used for 3-D recognition, respectively [50], [51]. Fig. 23(a)–(b) and Fig. 23(c)–(d) represent the reconstructed images obtained by use of on axis phase-shift digital holography and by use of one-shot on axis digital holography, respectively. They are all reconstructed by use of  $2048 \times 2048$  pixels. For the one-shot on axis scheme, the reconstructed image quality degrades due to the presence of the conjugate image term. However, 3-D object recognition is still possible. The direct use of the hologram in 3-D object recognition is practical in terms of faster processing time. Fig. 24 represents the 3-D correlation experimental results. Fig. 24(a) and 24(b) show the autocorrelation and cross correlation, respectively, which are obtained by using multiple exposure on axis phase-shift digital holography. Fig. 24(c) and 24(d) illustrate the autocorrelation and cross correlation, respectively, which are obtained by using one-shot on axis digital holography. For both cases, a hologram window with size  $256 \times 256$  pixels was used. As can be seen, the results show that one-shot on axis digital holography provides a reasonable capability for 3-D object recognition. The reason for the recognition capability of the proposed method is that the matched filter includes both information about the real

image and its conjugate term. The recognition results are similar to the phase-shift method. One of the benefits of the proposed one-shot approach is that the recognition system is extremely robust to external noise factors such as severe vibration and ambient fluctuation, which are inevitable difficulties for conventional phase-shift based recognition systems. Additionally, since only one hologram is used for 3-D recognition, the one-shot technique permits real-time recognition.

## VII. CONCLUSION

In this paper, various uses of digital holograms for 3-D display and 3-D information processing have been presented. The principles and properties of digital holography were first recalled, such as the possibility to reconstruct various views of the recorded objects. The application of these properties to 3-D imaging were then discussed. It was demonstrated that digital holograms permit either an optical or a digital reconstruction of the 3-D object. Moreover, digital holograms also have to be stored and transmitted. Various techniques to compress and encrypt 3-D information in the form of digital holograms were therefore presented. It was shown that the particular properties of holograms make it necessary to adapt the traditional compression algorithms used for regular images. In addition, several encryption schemes using phase masks as keys were described. The encryption can be realized by optical or digital means. Finally, the application of digital holography to the problem of 3-D object recognition was discussed. Various techniques were presented that allow one to achieve shift- and rotation-tolerant recognition, as well as an estimation of the orientation of the object. Also, 3-D object recognition using one-shot on axis digital holography was described. This technique requires a single exposure and thus makes the recording system less noise-sensitive and also usable in real time. All of the presented techniques show that digital holography provides a very complete solution to many problems of 3-D imaging and 3-D information processing.

## ACKNOWLEDGMENT

The authors would like to thank Dr. A. Castro from the National Institute for Astrophysics, Optics and Electronics, Puebla, Mexico, for her collaboration on distortion tolerant 3-D object recognition.

## REFERENCES

- [1] G. Lippmann, "La photographie intégrale," *Comptes-Rendus Academie des Sciences*, vol. 146, pp. 446–451, 1908.
- [2] D. Gabor, "A new microscopic principle," *Nature*, vol. 161, pp. 777–778, 1948.
- [3] B. Javidi and F. Okano, Eds., *Three-Dimensional Television, Video, and Display Technologies*. Berlin, Germany: Springer-Verlag, 2002.
- [4] J. W. Goodman and R. W. Lawrence, "Digital image formation from electronically detected holograms," *Appl. Phys. Lett.*, vol. 11, pp. 77–79, 1967.
- [5] A. Macovski, S. D. Ramsey, and L. F. Schaefer, "Time-lapse interferometry and contouring using television systems," *Appl. Opt.*, vol. 10, pp. 2722–2727, 1971.
- [6] K. Creath, "Phase-shifting speckle interferometry," *Appl. Opt.*, vol. 24, pp. 3053–3058, 1985.
- [7] L. Onural and P. D. Scott, "Digital decoding of in-line holograms," *Opt. Eng.*, vol. 26, pp. 1124–1132, 1987.

- [8] U. Schnars, "Direct phase determination in hologram interferometry with use of digitally recorded holograms," *J. Opt. Soc. Amer. A*, vol. 11, pp. 2011–2015, 1994.
- [9] U. Schnars and W. P. O. Jüptner, "Direct recording of holograms by a CCD target and numerical reconstruction," *Appl. Opt.*, vol. 33, pp. 179–181, 1994.
- [10] R. W. Kronrod, N. S. Merzlyakov, and L. P. Yaroslavskii, "Reconstruction of a hologram with a computer," *Sov. Phys. Tech. Phys.*, vol. 17, pp. 333–334, 1972.
- [11] G. Pedrini, S. Schedin, and H. Tiziani, "Lensless digital holographic interferometry for the measurement of large objects," *Opt. Commun.*, vol. 171, pp. 29–36, 1999.
- [12] Y. Takaki and H. Ohzu, "Fast numerical reconstruction technique for high-resolution hybrid holographic microscopy," *Appl. Opt.*, vol. 38, pp. 2204–2211, 1999.
- [13] F. Dubois, L. Joannes, and J.-C. Legros, "Improved three-dimensional imaging with a digital holography microscope with a source of partial spatial coherence," *Appl. Opt.*, vol. 38, pp. 7085–7094, 1999.
- [14] E. Cuche, P. Marquet, and C. Depeursinge, "Simultaneous amplitude contrast and quantitative phase-contrast microscopy by numerical reconstruction of Fresnel off axis holograms," *Appl. Opt.*, vol. 38, pp. 6994–7001, 1999.
- [15] T. Kreis, "Digital holographic interferometry," in *Trends in Optical Nondestructive Testing and Inspection*, P. K. Rastogi and D. Inaudi, Eds. Amsterdam, Netherlands: Elsevier Science, 2000, pp. 113–128.
- [16] T. Nomura and B. Javidi, "Securing information by use of digital holography," *Opt. Lett.*, vol. 25, pp. 28–30, 2000.
- [17] C. Wagner, W. Osten, and S. Seebacher, "Direct shape measurement by digital wavefront reconstruction and multi-wavelength contouring," *Opt. Eng.*, vol. 39, pp. 79–85, 2000.
- [18] M. Jacquot, P. Sandoz, and G. Tribillon, "High resolution digital holography," *Opt. Commun.*, vol. 190, pp. 87–94, 2001.
- [19] S. Grilli, P. Ferraro, S. De Nicola, A. Finizio, G. Pierattini, and R. Meucci, "Whole optical wavefields reconstruction by digital holography," *Opt. Exp.*, vol. 9, pp. 294–302, 2001.
- [20] X. Lei, P. Xiaoyuan, M. Jianmin, and A. K. Asundi, "Studies of digital microscopic holography with applications to microstructure testing," *Appl. Opt.*, vol. 40, pp. 5046–5052, 2001.
- [21] G. Pedrini and H. J. Tiziani, "Short-coherence digital microscopy by use of a lensless holographic imaging system," *Appl. Opt.*, vol. 41, pp. 4489–4496, 2002.
- [22] S. De Nicola, P. Ferraro, A. Finizio, and G. Pierattini, "Wave front reconstruction of Fresnel off axis holograms with compensation of aberrations by means of phase-shifting digital holography," *Opt. Laser Eng.*, vol. 37, pp. 331–340, 2002.
- [23] J. H. Massig, "Digital off axis holography with a synthetic aperture," *Opt. Lett.*, vol. 27, pp. 2179–2181, 2002.
- [24] H. J. Caulfield, Ed., *Handbook of Optical Holography*. London, U.K.: Academic, 1979.
- [25] J. H. Bruning, D. R. Herriott, J. E. Gallagher, D. P. Rosenfeld, A. D. White, and D. J. Brangaccio, "Digital wavefront measuring interferometer for testing optical surfaces and lenses," *Appl. Opt.*, vol. 13, pp. 2693–2703, 1974.
- [26] I. Yamaguchi and T. Zhang, "Phase-shifting digital holography," *Opt. Lett.*, vol. 22, pp. 1268–1270, 1997.
- [27] E. Tajahuerce, O. Matoba, and B. Javidi, "Shift-invariant three-dimensional object recognition by means of digital holography," *Appl. Opt.*, vol. 40, pp. 3877–3886, 2001.
- [28] O. Matoba, T. J. Naughton, Y. Frauel, N. Bertaux, and B. Javidi, "Real-time-three-dimensional object reconstruction by use of a phase-encoded digital hologram," *Appl. Opt.*, vol. 41, pp. 6187–6192, 2002.
- [29] T. J. Naughton, J. B. McDonald, and B. Javidi, "Efficient compression of Fresnel fields for Internet transmission of three-dimensional images," *Appl. Opt.*, vol. 42, pp. 4758–4764, 2003.
- [30] T. J. Naughton and B. Javidi, "Compression of encrypted three-dimensional objects using digital holography," *Opt. Eng.*, vol. 43, pp. 2233–2238, 2004.
- [31] T. Nomura, A. Okazaki, M. Kameda, Y. Morimoto, and B. Javidi, "Digital holographic data reconstruction with data compression," *Proc. SPIE*, vol. 4471, pp. 235–242, 2001.
- [32] T. J. Naughton, Y. Frauel, B. Javidi, and E. Tajahuerce, "Compression of digital holograms for three-dimensional object reconstruction and recognition," *Appl. Opt.*, vol. 41, pp. 4124–4132, 2002.



- [33] E. Tajahuerce and B. Javidi, "Encrypting three-dimensional information with digital holography," *Appl. Opt.*, vol. 39, pp. 6595–6601, 2000.
- [34] O. Matoba and B. Javidi, "Optical retrieval of encrypted digital holograms for secure real-time display," *Opt. Lett.*, vol. 27, pp. 321–323, 2002.
- [35] —, "Secure three-dimensional data transmission and display," *Appl. Opt.*, vol. 43, pp. 2285–2291, 2004.
- [36] B. Javidi and E. Tajahuerce, "Three-dimensional object recognition by use of digital holography," *Opt. Lett.*, vol. 25, pp. 610–612, 2000.
- [37] Y. Frauel, E. Tajahuerce, M.-A. Castro, and B. Javidi, "Distortion-tolerant 3-D object recognition using digital holography," *Appl. Opt.*, vol. 40, pp. 3887–3893, 2001.
- [38] Y. Frauel and B. Javidi, "Neural network for three-dimensional object recognition based on digital holography," *Opt. Lett.*, vol. 26, pp. 1478–1480, 2001.
- [39] Y. Frauel, E. Tajahuerce, O. Matoba, A. Castro, and B. Javidi, "Comparison of passive ranging integral imaging and active imaging digital holography for three-dimensional object recognition," *Appl. Opt.*, vol. 43, pp. 452–462, 2004.
- [40] B. M. Hennelly and J. T. Sheridan, "Fast numerical algorithm for the linear canonical transform," *JOSA A*, vol. 22, pp. 928–937, 2005.
- [41] D. A. Huffman, "A method for the construction of minimum redundancy codes," *Proc. IRE*, vol. 40, pp. 1098–1101, 1952.
- [42] J. Ziv and A. Lempel, "A universal algorithm for sequential data compression," *IEEE Trans. Inf. Theory*, vol. IT-23, no. 3, pp. 337–343, May 1977.
- [43] T. A. Welch, "A technique for high performance data compression," *IEEE Computer*, vol. 17, no. 6, pp. 8–19, Jun. 1984.
- [44] M. Burrows and D. J. Wheeler, "A block-sorting lossless data compression algorithm," Digital Systems Research Center Tech. Rep. 124, 1994.
- [45] J. W. Goodman and A. M. Silvestri, "Some effects of Fourier domain phase quantization," *IBM J. Res. Develop.*, vol. 14, pp. 478–484, 1970.
- [46] W. J. Dallas and A. W. Lohmann, "Phase quantization in holograms—depth effects," *Appl. Opt.*, vol. 11, pp. 192–194, 1972.
- [47] J. W. Goodman, *Introduction to Fourier Optics*, 2nd ed. New York: McGraw-Hill, 1996.
- [48] D. Casasent, "Unified synthetic discriminant function computational formulation," *Appl. Opt.*, vol. 23, pp. 1620–1627, 1984.
- [49] B. Javidi, "Nonlinear joint power spectrum based optical correlation," *Appl. Opt.*, vol. 28, pp. 2358–2367, 1989.
- [50] B. Javidi and D. Kim, "3-D object recognition using single exposure on axis digital holography," *Opt. Lett.*, vol. 30, pp. 236–238, 2005.
- [51] D. Kim and B. Javidi, "Distortion-tolerant 3-D object recognition by using single exposure on axis digital holography," *Opt. Express*, vol. 12, pp. 5539–5548, 2004.



**Yann Frauel** received the M.S. degree in optics from the École Supérieure d'Optique-SupOptique, Orsay, France, in 1995 and the Ph.D. degree in optics and photonics in 1999 from the Institut d'Optique-Université Paris XI, Orsay.

In 1995–1996, he worked for one year with the French Atomic Commission (CEA), Saclay, France, as a Military Assistant Engineer. In 2000, he held a five month postdoctoral position with the Department of Engineering of Cambridge University, Cambridge, U.K. In 2000–2001,

he worked for 18 months as an Associate Researcher with the Electrical and Computer Engineering Department of the University of Connecticut, Storrs. Since 2003, he has been an Associate Researcher with the Instituto de Investigaciones en Matemáticas Aplicadas y en Sistemas, Universidad Nacional Autónoma de México, Mexico City. His current research interests include three-dimensional acquisition and processing, pattern recognition and computer vision.



**Thomas J. Naughton** received the B.Sc. degree (double honors) in computer science and experimental physics from the National University of Ireland, Maynooth (formerly St. Patrick's College), Maynooth, Ireland, in 1995.

He has worked at Space Technology (Ireland) Ltd. and has been a visiting scholar at the Department of Radioelectronics, Czech Technical University, Prague, and the Department of Electrical and Computer Engineering, University of Connecticut, Storrs. He is currently a Lecturer in the Department of Computer Science, National University of Ireland, Maynooth. In this department, he leads research groups in optical information processing, computer theory (optical and biological models of computation), distributed computing, and bioinformatics.

Mr. Naughton is a member of the Association for Computing Machinery (ACM), the Optical Society of America (OSA), and SPIE.



**Osamu Matoba** received the Dr.Eng. degree in applied physics from Osaka University, Osaka, Japan, in 1996.

He was a Research Associate at Institute of Industrial Science, University of Tokyo, from 1996 to 2002. He is now an Associate Professor in the Department of Computer and Systems Engineering, Kobe University. His interests are in optical and digital processing of three-dimensional objects, terabyte holographic memory, and optical security.

Dr. Matoba is a member of the Optical Society of America (OSA), SPIE, the Optical Society of Japan, and the Japan Society of Applied Physics.



**Enrique Tajahuerce** received the B.S. and Ph.D. degrees in physics from the University of Valencia, Valencia, Spain, in 1988 and 1998, respectively.

From 1989 to 1992, he was a researcher in the Instituto Tecnológico de Óptica (AIDO), Valencia. Since 1992, he has been a member of the Departament de Ciències Experimentals in the University Jaume I, Castelló, Spain, where he is currently an Associate Professor. He had a research stay with the Electrical and Computer

Engineering Department in the University of Connecticut, Storrs, from 1999 to 2000. His research interests include optical image processing, diffractive optics and digital holography.

Dr. Tajahuerce is a member of SPIE, the Optical Society of America (OSA), and the Sociedad Española de Óptica (SEDO).



**Bahram Javidi** (Fellow, IEEE) received the B.S. degree in electrical engineering from George Washington University, Washington, D.C., and the M.S. and Ph.D. degrees in electrical engineering from Pennsylvania State University, University Park.

He is Board of Trustees Distinguished Professor at the University of Connecticut, Storrs. He has supervised over 80 masters and doctoral graduate students, postdoctoral students, and visiting professors during his academic career.

He has published over 200 technical articles in major journals. He has published over 230 conference proceedings, including over 90 invited conference papers, and 60 invited presentations. His papers have been cited over 2600 times, according to the citation index of *WEB of Science*. His papers have appeared in *Physics Today* and *Nature*, and his research has been cited in the *Frontiers in Engineering Newsletter*, published by the National Academy of Engineering, *IEEE Spectrum*, *Science*, *New Scientist*, and *National Science Foundation Newsletter*. He has completed several books including, *Optical Imaging Sensors and Systems for Homeland Security Applications* (Springer, 2005); *Optical and Digital Techniques*

*For Information Security* (Springer, 2005); *Image Recognition: Algorithms, Systems, and Applications* (Marcel Dekker, 2002); *Three Dimensional Television, Video, and Display Technologies* (Springer-Verlag, 2002); *Smart Imaging Systems* (SPIE Press, 2001); *Real-Time Optical Information Processing* (Academic Press, 1994), *Optical Pattern Recognition* (SPIE Press, 1994). He is currently the Editor in Chief of the Springer Verlag series on Advanced Science and Technologies for Security Applications. He has served as topical editor for Springer-Verlag, Marcel Dekker publishing company, *Optical Engineering Journal*, and IEEE/SPIE Press Series on Imaging Science and Engineering. He has held visiting positions during his sabbatical leave at Massachusetts Institute of Technology, United States Air Force Rome Lab at Hanscom Base, and Thomson-CSF Research Labs in Orsay, France. He is a consultant to industry in the areas of optical systems, image recognition systems, and 3-D optical imaging systems. He has active research collaborations with numerous universities and industries in the United States, Japan, South Korea, Italy, Germany, France, Ireland, United Kingdom, Egypt, Israel, Spain, and Mexico.

Dr. Javidi is a Fellow of the Optical Society of America (OSA) and Fellow of the International Society for Optical Engineering (SPIE). He was awarded the Dennis Gabor Award in Diffractive Wave Technologies by the SPIE in

2005. He was the recipient of the IEEE Lasers and Electro-Optics Society Distinguished Lecturer Award twice in 2003 and 2004. He has been awarded the University of Connecticut Board Of Trustees Distinguished Professor Award, the School Of Engineering Distinguished Professor Award, University of Connecticut Alumni Association Excellence in Research Award, the Chancellor's Research Excellence Award, and the first Electrical and Computer Engineering Department Outstanding Research Award. In 1990, the National Science Foundation named him a Presidential Young Investigator. He has served as the Chairman of the IEEE Lasers and Electro-Optics (LEOS) Technical Committee on Electro-Optics Sensors and Systems, member of the IEEE Neural Networks Council, Chairman of the Optics in Information System Working Group of Optical Engineering Society (SPIE), and Chair of the OSA Image Recognition technical Group. He has served on the program committees of more than two dozens international meetings on information systems sponsored by IEEE, OSA, SPIE, and ICO. He was awarded the IEEE Best Journal Paper Award from IEEE TRANSACTIONS ON VEHICULAR TECHNOLOGY in 2002. He is on the editorial board of the new IEEE JOURNAL OF DISPLAY TECHNOLOGIES.